Estimating the time-varying periodicity of epileptiform discharges in the electroencephalogram

John M. O' Toole,
Begoña García Zapirain
DeustoTech-LIFE,
University of Deusto,
Spain
email: j.otoole@deusto.es and mbgarciazapi@deusto.es

Iratxe Maestro Saiz,
Alina Beatriz Anaya Chen,
and Izaskun Yurrebaso Santamaría
Servicio de Neurofisiología Clínica,
Cruces Hospital,
Baracaldo, Spain

***Abstract*—Periodic lateralized epileptiform discharges (PLEDs) are EEG waveforms that can occur after brain injury or disease. The time-varying periodicity, or instantaneous frequency, of the PLEDs is a potentially important prognostic feature. Estimating the instantaneous frequency, however, is difficult because of the concurrent presence of background activity and artefacts. Here we present a method to enhance the instantaneous frequency features in the joint time–frequency domain. The procedure 1) enhances the PLED spikes in the time-domain using a simple energy operator; 2) transforms to the time–frequency domain using a separable-kernel distribution; and 3) uses a homomorphic filtering approach, within the time–frequency domain, to remove spectral modulation. Existing methods for instantaneous-frequency estimation are then applied to this enhanced time–frequency distribution. We show working examples with EEG epochs but have yet to test the method over an entire EEG database.**

I. INTRODUCTION

The electroencephalogram (EEG) can provide important diagnostic and prognostic information to the clinician. The EEG, which records electrical activity on the scalp using an array of electrodes, is routinely used in clinical settings to assess brain injury or brain disease [1]. Periodic lateralized epileptiform discharges (PLEDs) is the name given to a heterogeneous class of EEG waveforms which repeat at almost periodic intervals [2]. Studies have shown that PLEDs may represent ictal activity [3], [4]. And EEG-ictal activity warrants prompt neuroprotective treatment [4]. But for PLEDs which do not represent ictal activity [5] then treatment is neither necessary nor appropriate [6]. Thus we propose two classes of PLEDs, ictal PLEDs and non-ictal PLEDs, and aim to extract signal processing features to discriminate between the two classes. The methods presented here are a preliminary analysis for this project. As already noted in previous studies, the time-varying periodicity is associated with different prognostic classes of PLEDs [4], [7]. This paper presents an approach to estimate this time-varying periodicity, or instantaneous frequency (IF), for PLEDs.

Many methods exist for estimating the IF of a signal [8]–[14]. Most of these methods assume that the signal is monocomponent, meaning there is only one frequency component in the time–frequency domain [8]–[10]. Yet PLEDs are not monocomponent signals. PLEDs are a series of almost-periodic spikes or pulses [2]. And these time-varying spike or pulse trains are signals with time-varying spectral harmonics [15], [16] and are thus multicomponent signals. Most IF estimation methods for multicomponent signals use a sequence of peaks in the time–frequency domain to estimate the IFs [12]–[14]. We found, however, that these methods are not suitable for our PLED signals as EEG background activity and artefacts make it difficult to estimate the correct peaks in the time–frequency domain. What we present in this paper is a pre-processing step for these multicomponent IF estimation methods [12]–[14]. Specifically, we aim to enhance the time-varying harmonic characteristics of the PLED waveforms in the presence of nonstationary EEG background activity and artefacts.

We present the following approach to emphasize the time-varying harmonic structure of the PLEDs signals. First, we enhance the peaks of the PLEDs waveforms by using the Teager–Kaiser energy operator [17]. This method enhances spike-like components [18]. Next, we transform this spike-enhanced signal to the time–frequency domain. To do so, we use a quadratic time–frequency distribution with a separable kernel [11]. For the slowly-varying harmonic signals most of the cross-term energy is suppressed for this kernel [13], [16]. To remove the spectral envelope of the time–frequency distribution, we apply a homomorphic filtering approach [19], [20]. Specifically, we use the nonlinear transform to deconvolve the modulating spectral envelope from the harmonic signal. The use of the $\log$ transform means the convolution can be expressed as an addition operation in the time–lag domain. In this log-transformed time–lag domain, we apply a high-pass filter to separate the harmonic signal from the modulating spectral energy signal. Suppressing the spectral modulation enables a more accurate estimate of the IF of the harmonic signal. This final time–frequency distribution shows enhanced time-varying harmonic components comparative to the distribution of the original EEG signal. As this is a preliminary study, we have yet to quantify the results with the IF estimation methods; instead we provide some examples using EEG signals with PLED waveforms.

978-1-4673-0382-8/12/$31.00 ©2012 IEEE

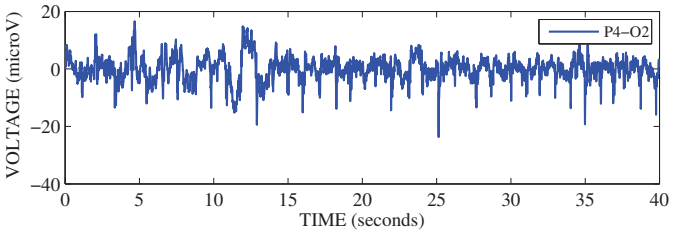

(a) 40 seconds EEG from channel P4–O2

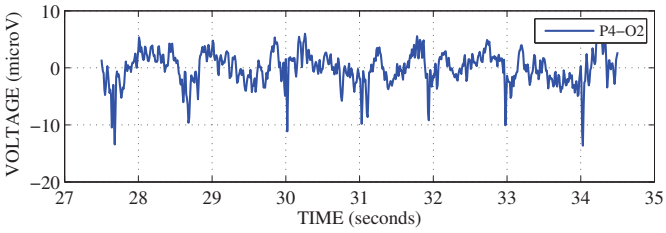

(b) a segment of the EEG epoch from (a)

Fig. 1. Segment of EEG signal with the periodic epilepiform waveforms known as PLEDs. In (b) note the varying morphology of the waveform with background activity between each discharge; also note the period between discharges is approximately 1 second.

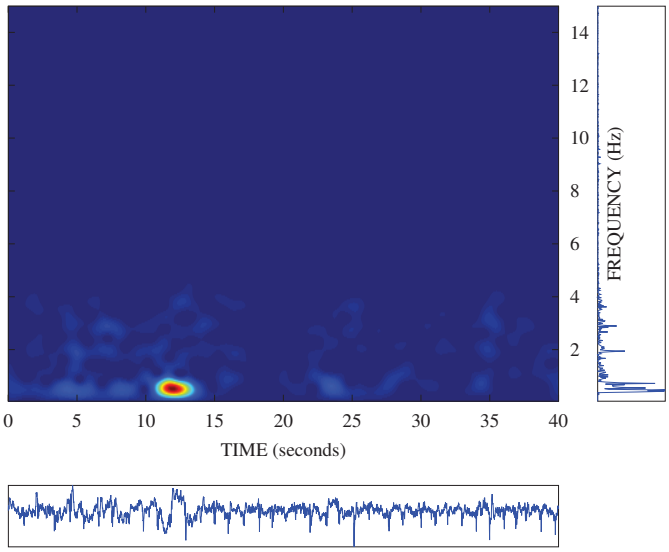

Fig. 2. Time–frequency distribution of the EEG signal in Fig 1. Note the artefact at 11–13 seconds dominates the entire distribution. The plot only displays the frequency range up to 15 Hz because little comparative signal energy resides above this frequency.

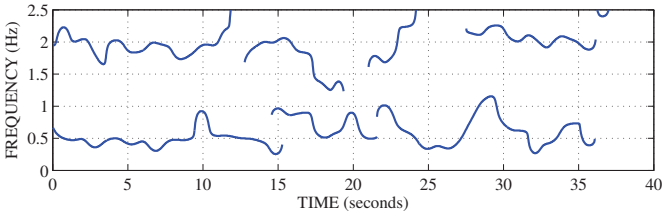

Fig. 3. Instantaneous frequency estimate using the time–frequency distribution in Fig. 2. The IF estimation method finds the peaks of the ridges in the distribution [13].

II. TIME–FREQUENCY ANALYSIS OF PERIODIC DISCHARGES

The PLED waveform can vary in morphology from one period to the next. Although the signal is defined as a periodic series of spikes or sharp waves [2], the varying morphology makes analysis difficult. In addition, other signal components are present in the signal, such as background activity or artefacts. Fig. 1 shows an example epoch of EEG with PLEDs. In Fig. 1(b) we can see the background activity between the PLEDs, which occur at intervals of approximately 1 second.

The approach we present here uses time–frequency analysis to estimate the time-varying periodicity, or IF, of the PLEDs. Because the IF is a function of both time t and frequency f, the time–frequency domain (t, f) is an obvious place to extract IF information [11]. Signal energy is represented as peaks in the time–frequency domain and continuous components are displayed as continuous ridges in this domain. Many IF estimation methods use the peak of these ridges as an IF estimate [12]–[14]. It is therefore important for an accurate IF estimate that the time–frequency domain displays a ridge or peak around the IF.

Experimenting with the EEG database with PLED waveforms, we found it difficult to achieve this goal. Even with the suppression of cross–terms [11] our time–frequency distribution was dominated by artefact energy making it difficult to extract the IF. (Cross–terms are explained in more detail in following Section II-C.) Fig. 2 shows a time–frequency distribution of the EEG signal from Fig. 1, where even with the removal of the high-energy artefact at 11–13 seconds, the slowly-varying IF of the PLED waveforms is hard to identify. Fig. 3 shows how a peak-extraction method [13] fails to estimate the IF of the PLED activity: we expect, from Fig. 1(b), an IF centred around 1 Hz.

A. Acquiring the EEG Data

The EEG data was recorded as part of a prospective and observational study to discriminate ictal from non-ictal PLEDs. The data was collected at a large teritary hospital (Cruces Hospital, Bilbao, Spain) by the members of the Clinical Neurophysiology Department (authors: IMS, ABAC, and IYS). The recordings were taken from the routine EEG exam for patients suspected of brain injury or disease. A Neurofax (Nihon Khoden, Rosbach, Germany) EEG machine, with 20 EEG channels in the standard 10–20 international placement system, was used to record the data. We analysed the data using a lateral-bipolar montage.

The first signal processing stage was to pre-process the data. We used a finite impulse response (FIR) filter with a bandpass region of 0.3–40 Hz. To preserve the time-domain features of the signal, we used a zero-phase filter using the forward–reverse method [21]. Next, we downsampled the signal from the original sampling rate of 500 Hz to 100 Hz. Lastly, large-amplitude artefacts were removed using the following threshold approach: if the EEG signal $s(t)$ at time instance t_0 is greater than a predefined threshold, then set this signal to zero and also the all adjecent samples within a small window

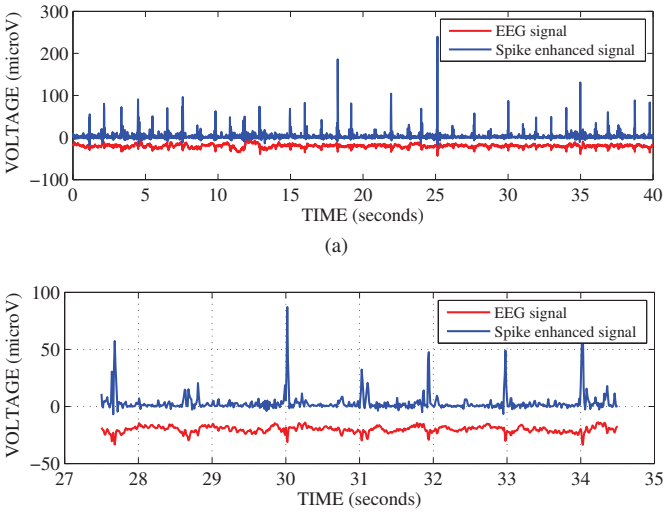

(b) a segment of the EEG epoch from (a)

Fig. 4. EEG signal from Fig. 1 after emphasising the spikes with high-pass filtering and applying the Teager–Kaiser energy operator. The original EEG signal (in red) is offset by -20 μV to aid clarity.

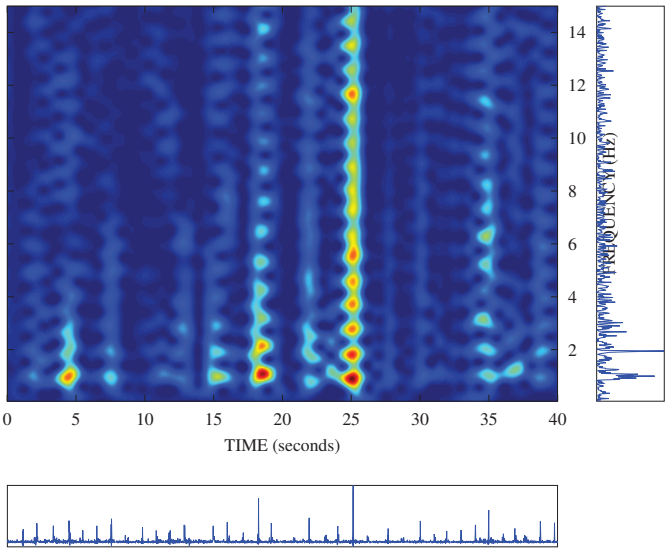

Fig. 5. Time–frequency distribution of EEG signal in Fig. 4 after Teager–Kaiser energy operation.

frame; that is, if $s(t_0) > \zeta$ at time t_0 then let $s(t_0 + \tau) = 0$ for $-L/2 \leq \tau \leq L/2$; and if $s(t_0) \leq \zeta$ then do nothing. We set ζ to 300 μVs and L to 5 seconds.

B. Emphasising Peaks of Epileptiform Discharges

To emphasis the peaks of the epileptiform discharges we use the Teager–Kaiser energy operator [17]. This simple method has been used for the analysis of many biomedical signals, including extracting spikes from EEG data [18]. The two stage process is as follows. First, we high-pass filter the signal, with a cutoff frequency of 3 Hz, to remove low frequency trends. Again, we use the zero-phase finite impulse response filter [21]. Then, we apply the energy operator [17] to the filtered (discrete) signal $s[n]$:

$$y[n] = s[n+1]^2 - s[n+2]s[n]. \tag{1}$$

Fig. 4 shows the EEG sample from Fig. 1 processed by this spike-emphasis approach. And Fig. 5 shows the time–frequency distribution of this spike-enhanced signal. Although the distribution now displays the spikes in time–frequency domain there is still a lack of continuous slowly-varying components to represent the IF of the PLEDs.

C. Design of the Time–Frequency Distribution

To aid the design process we start with a simple model of the signal and make some assumptions to simplify the analysis; we later justify these assumptions by testing with real signals. Lets first assume that the slowly time-varying harmonic signal can be modelled by a piecewise-linear frequency modulated (FM) signal with harmonic components [15], [16]. For one *piece* (segment) of this piecewise-linear FM signal, the signal is a linear FM signal with K harmonics,

$$x(t) = \sum_{q=1}^{K+1} \mathrm{e}^{\,\mathrm{j}2\pi t(qf_0 + \alpha t/2)} \tag{2}$$

Here f_0 represents the fundamental frequency and α the slope-constant of the linear FM signal. The Wigner–Ville distribution for an arbitrary, real-valued signal $x(t)$ is defined as

$$W_z(t,f) = \int_{-\infty}^{\infty} z(t+\tfrac{\tau}{2}) z^*(t-\tfrac{\tau}{2}) \mathrm{e}^{-\mathrm{j}2\pi\tau f} \mathrm{d}\tau$$

where the $z(t)$ is the analytic associate of $x(t)$ [11] and $z^*(t)$ is the conjugate operation. Assuming that the signal $x(t)$ in (2) is already an analytic signal, the Wigner–Ville distribution of this signal is [22], [23]

$$W_x(t,f) = \sum_{q=1}^{K+1} \delta[f - (qf_0 + \alpha t)] + W_{\text{cross-terms}}(t,f) \tag{3}$$

The Wigner–Ville distribution is an important distribution in the class of quadratic time–frequency distributions as it can resolve linear FM signals to time-varying delta functions, as shown in this equation [11]. These delta functions are ideal time–frequency representations for these signals. But there is also another component to the distribution known as the cross-terms; in (3) the cross-terms are in $W_{\text{cross-terms}}(t,f)$. These cross-terms create difficulty for signal interpretation and need to be suppressed, or ideally removed, before further signal analysis [11]. Minimising the effects of the cross-terms for our time–frequency method is the first task. Before describing the solution to this task we first present the second task.

The signal model in (2) produces a series of delta functions with equal amplitude in the time–frequency domain. Real EEG however has most of its energy concentrated around the lower frequencies [15], [24]. To incorporate this spectral shaping into our signal model $x(t)$ we modulate the spectrum of $x(t)$ with a low-pass function; this is equivalent to convolving in the time-domain with a function $h(t)$,

$$y(t) = x(t) * h(t)$$

For our analysis here we use the Gaussian function defined in time $h(t)$ and frequency $H(f)$ as

$$h(t;\sigma) = \mathrm{e}^{-t^2\sigma^2} \qquad (4)$$
$$H(f;\sigma) = \sqrt{\frac{\pi}{\sigma^2}}\mathrm{e}^{-(\pi f)^2/\sigma^2}$$

where σ controls the width of this window function. Assume that we set σ so that $H(f;\sigma)$ is a wide-band signal and $h(t;\sigma)$ is narrowband. Thus $H(f;\sigma)$ represents the spectral trend or envelope of the frequency-domain signal $Y(f)$. The Wigner–Ville distribution of $y(t)$ is now

$$W_y(t,f) = \bar{H}(f)\left[\sum_{q=1}^{K+1}\delta(f-[qf_0+\alpha t]) + W_{\text{cross-terms}}(t,f))\right] \underset{t}{*} \bar{h}(t) \qquad (5)$$

as [11]

$$W_y(t,f) = W_x(t,f) \underset{t}{*} W_h(t,f)$$

with

$$W_h(t,f) = \bar{h}(t)\bar{H}(f)$$

and

$$\bar{h}(t) = h(t;\frac{\sigma}{\sqrt{2}}); \qquad \bar{H}(f) = h(f;\frac{\sigma}{\sqrt{2}})$$

Thus in (5), the delta functions are now modulated with the low-pass function $\bar{H}(f)$. Also, the distribution $W_x(t,f)$ is convolved in time with the Gaussian function $\bar{h}(t)$. This convolution will smear the components in the time direction. Although (5) is a more realistic model of the PLEDs spike-train compared to (3), we would like our analysis to produce a time–frequency distribution closer to (3). Flattening the spectrum has been shown to improve signal analysis for particular EEG applications [25], [26]. Thus our second task is to suppress the spectral modulation of the signal in the time–frequency domain.

1) Task 1: Removing Cross-Terms: We would like to remove, or suppress, the cross-terms components in (3). This should, ideally, not be at the expense of also suppressing or smearing the auto-term components; in (3) the auto-terms are the delta functions. In practice, there is a trade-off between cross-term suppression and the preservation of auto-term resolution. The quadratic class of time–frequency distributions provides different options to suppress cross-terms whilst preserving the auto-terms for multicomponent signals. The class can be written as a function of the Wigner–Ville distribution as

$$\rho_z(t,f) = W_z(t,f) \underset{t}{*}\underset{t}{*} \gamma(t,f) \qquad (6)$$

where $\gamma(t,f)$ is known as the time–frequency kernel of the distribution $\rho_z(t,f)$. One study shows that lag-independent kernels, with $\gamma(t,f) = G(t)$, can give optimal suppression of cross-terms for stationary FM signals [27]. Because our test signal $x(t)$ here is nonstationary, we include a lag window [23]; now we have the separable kernel $\gamma(t,f) = G(t)M(f)$ which has been shown to be an effective kernel for suppressing kernels for slowly-varying harmonic signals [16], [23].

Using $\gamma(t,f) = G(t)M(f)$, and assuming all cross-terms are eliminated, we can rewrite (3) as

$$\rho_y(t,f) \approx \left[\bar{H}(f)\sum_{q=1}^{K+1} M(f-[qf_0+\alpha t])\right] \underset{t}{*} \bar{G}(t) \qquad (7)$$

where $\bar{G}(t) = G(t)\bar{h}(t)$. The approximation in (7) is exact only when all cross-terms are removed.

2) Task 2: Removing Spectral Modulation: By taking the inverse Fourier transform of $\rho_y(t,f)$ we get the time–lag domain (t,τ) [11]

$$K_y(t,\tau) = \underset{f\to\tau}{\mathcal{F}}^{-1}\{\rho_y(t,f)\} = \bar{h}(\tau) \underset{\tau}{*} \left[\sum_{q=1}^{K+1} m(\tau)\mathrm{e}^{\,\mathrm{j}2\pi\tau(qf_0+\alpha t)}\right] \underset{t}{*} \bar{G}(t) \qquad (8)$$

where $\mathcal{F}^{-1}$ represents the inverse Fourier transform as frequency f is transformed to lag value τ. Although $\bar{h}(\tau)$ is a narrowband signal centred on the origin $\tau = 0$, it is not easy to remove $\bar{h}(\tau)$ from $K_y(t,\tau)$ as $\bar{h}(\tau)$ is convolved with the auto–terms in $K_y(t,\tau)$. Note also that it is not easy to remove this modulating term in the time–frequency domain in (7) either, as the function $\bar{H}(f)$ is a wide-band signal.

We now use the concept of homomorphic filtering to deconvolve $\bar{h}(\tau)$ with the rest of the expression in (8). Homomorphic analysis uses a nonlinear function to transform a multiplication operation to an addition operation and then uses another transformation, in this case a Fourier transform, to transform to a domain where the two signals are separable [19]. Examples of applications using homomorphic analysis include speech and seismic applications [19], [20].

We apply a log transform to $\rho_y(t,f)$ in (7) before taking the inverse Fourier transform to convert the convolution operation in (8) to an addition operation:

$$R_y(t,\tau) = \underset{f\to\tau}{\mathcal{F}}^{-1}\{\log\rho_y(t,f)\} = \underset{f\to\tau}{\mathcal{F}}^{-1}\left\{\log\left(\sum_{q=1}^{K+1} M\left[f-(qf_0+\alpha t)\right] \underset{t}{*} \bar{G}(t)\right)\right\} + \underset{f\to\tau}{\mathcal{F}}^{-1}\left\{\log\bar{H}(f)\right\} \qquad (9)$$

To simplify analysis we do not create a separate *quefrency* domain [19] but keep the terminology of the lag domain τ; but note that $R_y(t,f)$ is not equal to $K_y(t,\tau)$.

Simple filtering methods will separate the two terms in (9): the first term is a broadband signal and the second term is a narrowband signal centred around the origin. Thus we multiply $R_y(t,\tau)$ with a high-pass function $l(\tau)$. After this filtering operation we transform back to the time–frequency domain and apply the inverse $\log$ transform:

$$\eta_y(t,f) = \mathrm{e}^{\underset{\tau\to f}{\mathcal{F}}\{R_y(t,\tau)l(\tau)\}}. \qquad (10)$$

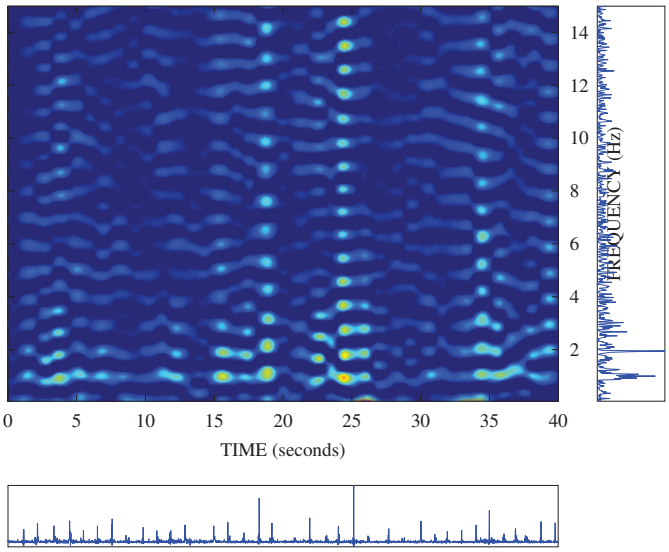

Fig. 6. Time–frequency distribution of EEG signal in Fig. 4 using the homomorphic method to spread the spectral content.

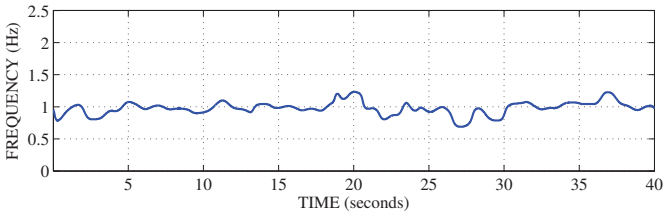

Fig. 7. Instantaneous frequency extracted from the time–frequency distribution in Fig. 6 using the peak-picking method in [13]. The plots shows only the fundamental frequency.

Assuming that the term $\mathcal{F}^{-1}\{\log \bar{H}(f)\}$ is removed by the operation $R_y(t,\tau)l(\tau)$ and that this windowing operation does no have a significant effect on $\mathcal{F}\{\log\left(\sum_{q=1}^{K+1} M\left[f-(qf_0+\alpha t)\right] \underset{t}{*} \bar{G}(t)\right)\}$ then

$$\eta_y(t,f) \approx \sum_{q=1}^{K+1} M\left[f-(qf_0+\alpha t)\right] \underset{t}{*} \bar{G}(t)$$

Thus, $\eta_y(t,f)$ is (approximately) equal to the desired distribution

$$\rho_x(t,f) = \sum_{q=1}^{K+1} \delta\left[f-(qf_0+\alpha t)\right]$$

with the addition of smearing in the time and frequency from the functions $\bar{G}(t)$ and $M(f)$.

Fig. 6 shows the EEG spike-enhanced signal from Fig. 5 but here the distribution is generated using this proposed homomorphic approach. From this time–frequency representation we can use any of the previously proposed methods to extract the IF. In Fig. 7 we use method in [13] to estimate the fundamental frequency of the EEG signal.

3) Numerical Implementation: Implementing the distribution with a discrete, finite-length signal $y[n]$ necessities some deviation from the proceeding analysis.

First, we have the problem of using the *log* of a time–frequency distribution: TFDs are not always positive valued and often contain zero-values. To avoid singularities and complex numbers, we threshold all values in the distribution which are below zero to zero; and we add a small bias before computing the log the distribution. Thus we use

$$\log\left\{T_0(\rho_y[n,k]) + \epsilon\right\}$$

instead of $\log \rho_y[n,k]$; $[n,k]$ are the discrete-time and discrete-frequency variables of (t,f) [28]; and T_0 is threshold function: $T_0(x) = 0$ if $x < 0$ and $T_0(x) = x$ if $x >= 0$. Although singularities can be avoid by using a very small value for ϵ, any values of $\rho_y[n,k]$ close to this singularity will produce very large negative values for $\log \rho_y[n,k]$. This proximity to the singularity is problematic for time–frequency distributions where often most of the time–frequency plane will have values close to zero. To avoid these singularity spikes in the log transform, we set $\epsilon = \mu \max_{(t,f)} \rho_y[n,k]$. In our analysis with the EEG we used $\mu = 0.3$.

Second, to enable analysis without constraining the duration of the EEG epoch to short lengths, we use the algorithms in [23] to control the level of oversampling for the discrete time–frequency distribution. For our tests we used a distribution of dimension $N_{\text{time}} \times N_{\text{freq}} = 8\ 192 \times 512$ for the signal of length $N = 4\ 000$; these algorithms enable computation of time–frequency distributions without exceeding the memory limit for our desktop computer.

4) Summary of Method: The method to form the time–frequency distribution is as follows:

Step 1 high-pass filter with a cut-off of 3 Hz to filter;

Step 2 apply the Teager–Kaiser operator in (1) to obtain $y(t)$;

Step 3 generate a time–frequency distribution $\rho_y(t,f)$ in (6) with a separable kernel $\gamma(t,f) = G(t)M(f)$;

Step 4 inverse Fourier transform, using the nonlinear log transform, to the time–lag domain and multiply by the high-pass function $l(\tau)$

$$R_y(t,\tau) = \underset{f\to\tau}{\mathcal{F}}^{-1}\left\{\log\left(T_0[\rho_y(t,f)] + \epsilon\right)\right\} l(\tau)$$

Step 5 transform back to the time–frequency domain:

$$\eta_y(t,f) = \mathrm{e}^{\underset{\tau\to f}{\mathcal{F}}\{R_y(t,\tau)\}}.$$

Step 6 extract the IF (instantaneous frequency) from $\eta_y(t,f)$ by tracking the peak of time–frequency components [12]–[14].

The parameters used for discrete time–frequency distributions were as follows. The lag-function $m(\tau)$ was a Hanning window of (discrete) length $4f_s$, where f_s is the sampling frequency (100 Hz); and the Doppler-function $g(\nu)$ was a Hamming window of (discrete) length $f_s 1.75/N$, where N is the length of the discrete signal $y[n]$. The high-pass filter $l(\tau)$ was a Tukey window, shifted from the origin by the length of the positive lag axis, with a parameter value of 0.25.

III. DISCUSSION

The time–frequency distribution presented here suppresses the spectral modulation on a time-varying basis: that is, the filtering, or *liftering* operation [19], is achieved in the time-varying lag (time–lag) domain. We could apply the same liftering procedure to the entire $y(t)$ signal before the time–frequency analysis. There are some limitations with this approach however. First, generating a complex cepstrum is problematic for a noisy signal with an arbitrary phase spectrum [19], [20]. And second, although we can achieve a flat magnitude spectrum, the method does not preserve the features of the signal in the time-domain. The time–frequency method we use here is a more robust approach because the time–frequency domain is real-valued and therefore we do not use the complex cepstrum [19], [20]; and also we need not preserve the time-domain features, as we use only the (time-varying) spectrum in the time–frequency distribution.

Alternative methods to our time–frequency approach may also be applicable to estimate the IF of the PLED waveform. For example, methods to estimate instantaneous heart-rate from electrocardiogram signals [29] or methods to estimate the fundamental frequency of speech signals [30] may be adapted to PLED waveforms.

As this is only a preliminary analysis there is still much work to do. We next need to quantify the performance of our proposed method at estimating the IF of the PLED waveforms, possibly using simulated EEG signals with known IF laws. Then we will test the efficacy of the estimated IF as a feature to discriminate between ictal and non-ictal PLEDs.

REFERENCES

[1] S. Seidel, S. Aull-Watschinger, and E. Pataraia, "The yield of routine electroencephalography in the detection of incidental nonconvulsive status epilepticus—A prospective study." *Clinical Neurophysiology*, vol. 123, pp. 459–462, Jul. 2011.

[2] G. Chatrian, "The significance of periodic lateralized epileptiform discharges in EEG: An electrographic, clinical and pathological study,," *Electroencephalography and Clinical Neurophysiology*, vol. 17, no. 2, pp. 177–193, Aug. 1964.

[3] D. J. Chong and L. J. Hirsch, "Which EEG patterns warrant treatment in the critically ill? Reviewing the evidence for treatment of periodic epileptiform discharges and related patterns," *Journal of Clinical Neurophysiology*, vol. 22, no. 2, 2005.

[4] J. R. Hughes, "Periodic lateralized epileptiform discharges: Do they represent an ictal pattern requiring treatment?" *Epilepsy & Behavior*, vol. 18, no. 3, pp. 162–5, Jul. 2010.

[5] B. Pohlmann-Eden, D. B. Hoch, J. I. Cochius, and K. H. Chiappa, "Periodic lateralized epileptiform discharges—a critical review," *Journal of Clinical Investigation*, vol. 13, no. 6, pp. 519–530, 1996.

[6] R. Alroughani, M. Javidan, A. Qasem, and N. Alotaibi, "Non-convulsive status epilepticus; the rate of occurrence in a general hospital." *Seizure*, vol. 18, no. 1, pp. 38–42, Jan. 2009.

[7] I. García-Morales, M. Teresa Garcia, L. Galán-Dávila, C. Gómez-Escalonilla, P. Rosana Saiz-Díaz, Antonio Martínez-Salio, and J. A. T. De La Peña, "Periodic lateralized epileptiform discharges: etiology, clinical aspects, seizures, and evolution in 130 patients," *Journal of Clinical Neurophysiology*, vol. 19, no. 2, pp. 172–177, 2002.

[8] B. Boashash, "Estimating and interpreting the instantaneous frequency of a signal—part 1: fundamentals," *Proc. IEEE*, vol. 80, no. 4, pp. 520–538, 1992.

[9] V. Katkovnik and L. Stankovic, "Instantaneous frequency estimation using the Wigner distribution with varying and data-driven window length," *IEEE Trans. Signal Process.*, vol. 46, no. 9, pp. 2315–2325, 1998.

[10] P. O' Shea, "A fast algorithm for estimating the parameters of a quadratic FM signal," *IEEE Trans. Signal Process.*, vol. 52, no. 2, pp. 385–393, 2004.

[11] B. Boashash, Ed., *Time–Frequency Signal Analysis and Processing: A Comprehensive Reference*. Oxford, UK: Elsevier, 2003.

[12] R. McAulay and T. Quatieri, "Speech analysis/synthesis based on a sinusoidal representation," *IEEE Trans. Acoust., Speech, Signal Process.*, vol. 34, no. 4, pp. 744–754, Aug. 1986.

[13] L. Rankine, M. Mesbah, and B. Boashash, "IF estimation for multicomponent signals using image processing techniques in the time–frequency domain," *Signal Process.*, vol. 87, no. 6, pp. 1234–1250, 2007.

[14] J. Lerga, V. Sucic, and B. Boashash, "An efficient algorithm for instantaneous frequency estimation of nonstationary multicomponent signals in low SNR," *EURASIP J. Adv. Signal Process.*, vol. 2011, no. Article ID: 725189, pp. 1–16, 2011.

[15] L. Rankine, N. Stevenson, M. Mesbah, and B. Boashash, "A nonstationary model of newborn EEG." *IEEE Trans. Biomed. Eng.*, vol. 54, no. 1, pp. 19–28, Jan. 2007.

[16] J. M. O' Toole and B. Boashash, "Time–frequency detection of slowly varying periodic signals with harmonics: methods and performance evaluation," *EURASIP J. Adv. Signal Process.*, vol. 2011, no. Article ID 193797, pp. 1–16, 2011.

[17] J. Kaiser, "On a simple algorithm to calculate the 'energy' of a signal," in *IEEE Int. Conf. Acoustics, Speech, and Signal Process., ICASSP-90*. IEEE, 1990, pp. 381–384.

[18] S. Mukhopadhyay and G. C. Ray, "A new interpretation of nonlinear energy operator and its efficacy in spike detection." *IEEE Trans. Biomed. Eng.*, vol. 45, no. 2, pp. 180–7, Feb. 1998.

[19] D. Childers, D. Skinner, and R. Kemerait, "The cepstrum: A guide to processing," *Proc. IEEE*, vol. 65, no. 10, pp. 1428–1443, 1977.

[20] T. Quatieri, *Discrete-time speech signal processing: principles and practice*. Upper Saddle River, New Jersey: Prentice Hall, 2002.

[21] A. V. Oppenheim and R. W. Schafer, *Discrete-Time Signal Processing*. Englewood Cliffs, NJ 07458: Prentice-Hall, 1999.

[22] G. F. Boudreaux-Bartels, "Mixed Time–Frequency Signal Transformations," in *The Transforms and Applications Handbook: Second Edition*, A. D. Poularikas, Ed. Boca Raton: CRC Press LLC, 2000, ch. 12.

[23] J. M. O' Toole, "Discrete quadratic time–frequency distributions: definition, computation, and a newborn electroencephalogram application," Ph.D. dissertation, School of Medicine, The University of Queensland, Nov. 2009. [Online]. Available: http://espace.library.uq.edu.au/view/UQ:185537

[24] N. J. Stevenson, M. Mesbah, G. B. Boylan, P. B. Colditz, and B. Boashash, "A nonlinear model of newborn EEG with nonstationary inputs," *Annals of Biomedical Engineering*, vol. 38, no. 9, pp. 3010–3021, Sep. 2010.

[25] P. Celka and P. Colditz, "A computer-aided detection of EEG seizures in infants: A singular-spectrum approach and performance comparison," *IEEE Trans. Biomed. Eng.*, vol. 49, no. 5, pp. 455–462, 2002.

[26] N. J. Stevenson, J. M. O'Toole, L. J. Rankine, G. B. Boylan, and B. Boashash, "A nonparametric feature for neonatal EEG seizure detection based on a representation of pseudo-periodicity." *Medical Engineering & Physics*, vol. in press, Sep. 2011.

[27] Z. Hussain and B. Boashash, "The T-class of time–frequency distributions: time-only kernels with amplitude estimation," *Journal of the Franklin Institute*, vol. 343, no. 7, pp. 661–675, Nov. 2006.

[28] J. M. O' Toole, M. Mesbah, and B. Boashash, "Improved discrete definition of quadratic time–frequency distributions," *IEEE Trans. Signal Process.*, vol. 58, no. 2, pp. 906–911, Feb. 2010.

[29] S. Dong, F. Xu, B. Lingwood, M. Mesbah, and B. Boashash, "R-wave: a comparative analysis of four methods using newborn piglet ECG," in *10th Int. Conf. on Information Science, Signal Processing and their Applications (ISSPA 2010)*, no. Isspa, Kuala Lumpur, 2010, pp. 320–323.

[30] C. Shahnaz, W.-P. Zhu, and M. Ahmad, "Pitch estimation based on a harmonic sinusoidal autocorrelation model and a time-domain matching scheme," *IEEE Trans. Audio, Speech, Language Process.*, vol. 20, no. 99, pp. 322–335, 2012.